Nuclear Science and Techniques (2025) 36:34
https://doi.org/10.1007/s41365-024-01631-x

New measurement of ^{63}Cu(γ, n)^{62}Cu cross-section using quasi-monoenergetic γ-ray beam

Zhi-Cai Li[1,2] · Zi-Rui Hao[2] · Qian-Kun Sun[3,4] · Yu-Long Shen[1] · Long-Xiang Liu[2] · Hang-Hua Xu[2] · Yue Zhang[2] · Pu Jiao[2,5] · Meng-Die Zhou[2,5] · Yu-Xuan Yang[3] · Sheng Jin[3,4] · Kai-Jie Chen[3] · Zhen-Wei Wang[3,4] · Shan Ye[6] · Xin-Xiang Li[1] · Chun-Wang Ma[5,7] · Hong-Wei Wang[2,3,4] · Gong-Tao Fan[2,3,4] · Wen Luo[1]

Received: 27 September 2024 / Revised: 2 November 2024 / Accepted: 29 November 2024 / Published online: 14 January 2025

Abstract
We present new data on the ^{63}Cu(γ, n) cross-section studied using a quasi-monochromatic and energy-tunable γ beam produced at the Shanghai Laser Electron Gamma Source to resolve the long-standing discrepancy between existing measurements and evaluations of this cross-section. Using an unfolding iteration method, ^{63}Cu(γ, n) data were obtained with an uncertainty of less than 4%, and the inconsistencies between the available experimental data were discussed. The γ-ray strength function of ^{63}Cu(γ, n) was successfully extracted as an experimental constraint. We further calculated the cross-section of the radiative neutron capture reaction ^{62}Cu(n, γ) using the TALYS code. Our calculation method enables the extraction of (n, γ) cross-sections for unstable nuclides.

Keywords ^{63}Cu(γ · n) reaction; Cross-section data; Quasi-monochromatic γ beam; Radiative neutron capture reaction

This work was supported by the National Key Research and Development Program (Nos. 2023YFA1606901 and 2022YFA1602400), National Natural Science Foundation of China (Nos. U2230133, 12275338, and 12388102), and Open Fund of the CIAE Key Laboratory of Nuclear Data (No. JCKY2022201C152).

✉ Gong-Tao Fan
fangt@sari.ac.cn

✉ Wen Luo
wenluo-ok@163.com

1 School of Nuclear Science and Technology, University of South China, Hengyang 421001, China

2 Shanghai Advanced Research Institute, Chinese Academy of Sciences, Shanghai 201210, China

3 Shanghai Institute of Applied Physics, Chinese Academy of Sciences, Shanghai 201800, China

4 University of Chinese Academy of Science, Beijing 100049, China

5 School of Physics, Henan Normal University, Xinxiang 453007, China

6 China Institute of Atomic Energy, Beijing 102413, China

7 Institute of Nuclear Science and Technology, Henan Academy of Sciences, Zhengzhou 450046, China

1 Introduction

^{62}Cu, which can be produced by the ^{63}Cu(γ, n) reaction, is a relatively short-lived β^+ emitter ($T_{1/2}$ = 9.67 min) suitable for positron emission tomography (PET) imaging. For example, [^{62}Cu]Cu para-toluene sulfonic acid methyl ester (PTSM) provides high-quality brain and heart images with PET, accurately delineating cerebral and myocardial perfusion in both animals and humans [1]. Accurate cross-sectional data for the ^{63}Cu(γ, n) reaction are required to guide the production of the ^{62}Cu isotope for medical purposes [2, 3]. Moreover, the ^{63}Cu(γ, n) reaction cross-section data can be applied to monitor the bremsstrahlung radiation [4] and LCS γ-ray [5] fluxes. In addition, the β^+ decay process of ^{62}Cu is an alternative pathway for the synthesis of the "iron group element" ^{62}Ni, and knowledge of the radiative neutron capture reaction ^{62}Cu(n, γ) can help us understand the nucleosynthesis of intermediate-mass elements, as shown in Fig. 1.

Over the past few decades, ^{63}Cu photoneutron reactions have been experimentally studied worldwide using electron accelerator-based bremsstrahlung radiation or positron annihilation in flight γ beam facilities [4, 6–11]. Cross-sectional data of ^{63}Cu(γ, n) and ^{63}Cu(γ, 2n) reactions were obtained

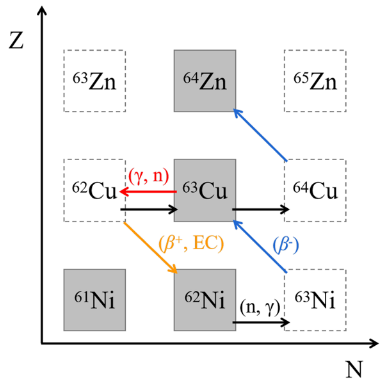

Fig. 1 (Color online) Nuclear reaction path around the Cu isotope

and subsequently evaluated by Varlamov et al. [12, 13]. However, discrepancies in the shapes, peak heights, and positions of these experimental and evaluated cross-sectional data curves were observed. Additionally, the peak widths of these curves were different [14]. These discrepancies must be resolved. For example, the experimental data of Fultz [7] were systematically 15% lower than those of Varlamov [12]. A recent article [15] reported significantly different peak values of 79.79 mb and 59±6 mb for the evaluated ^{63}Cu(γ, n) and experimental data, respectively [7]. Varlamov et al. [13] analyzed experimental ^{63}Cu(γ, 2n) data [7] using an experimental–theoretical procedure [16, 17], indicating the need for reasonable verification and correction of these data. Luo et al. [18] proposed a method for extracting the (γ, n) cross-sectional distribution of ~40 isotopes, including ^{63}Cu, using laser-induced γ activation and the isotope yield ratio.

Furthermore, owing to the extreme difficulty in obtaining the ^{62}Cu target, experimental data on the ^{62}Cu(n, γ) reaction are unavailable in any neutron energy range [14]. However, such data can be extracted indirectly from the cross-section of its inverse ^{63}Cu(γ, n) reaction, which requires accurate ^{63}Cu(γ, n) data with sufficiently small measurement uncertainty. Consequently, obtaining new data on the ^{63}Cu(γ, n) reaction and calculating the cross-section of the ^{62}Cu(n, γ) reaction are essential.

The Shanghai Laser Electron Gamma Source (SLEGS) is an energy-tunable laser Compton scattering (LCS) γ-ray source that provides meV γ beams for nuclear science and technology [19–21]. It was developed based on the inverse Compton scattering of 10.64 µm CO_2 laser photons from 3.5 GeV relativistic electrons in the storage ring of the Shanghai Synchrotron Radiation Facility (SSRF) [22, 23]. SLEGS delivers γ beams with energies of 0.66−21.1 MeV in the slant-scattering mode at scattering angles of 20–160° and at a maximum energy of 21.7 MeV in the back-scattering mode at 180°. The full-spectrum flux ranges from ~10^5 photons/s at 20° to ~10^7 photons/s at 180° [24, 25]. SLEGS provides a suitable experimental platform for conducting various types of photonuclear reaction experiments and is particularly suitable for experimental measurements of the (γ, n) and (γ, 2n) cross-sections in the giant dipole resonance (GDR) energy region.

In this study, we experimentally investigated the ^{63}Cu(γ, n) cross-section based on quasi-monochromatic and energy-tunable SLEGS γ beams. Using an unfolding iteration method, ^{63}Cu(γ, n) data were obtained within the energy range of 11.1 −19.7 MeV. Then, the γ-ray strength function (γSF) of the ^{63}Cu(γ, n) reaction was extracted, and the cross-section of its inverse reaction, ^{62}Cu(n, γ), was successfully calculated. The remainder of this paper is organized as follows. In Sect. 2, the experimental procedure used to measure the ^{63}Cu(γ, n) cross-section is described. In Sect. 3, the results of the monochromatic and unfolded ^{63}Cu(γ, n) cross-sections are presented. In Sect. 4, the inconsistency between the available experimental data from different laboratories is discussed, and the experimentally constrained γSF for the ^{63}Cu(γ, n) reaction and cross-sectional data of the inverse reaction, ^{62}Cu(n, γ), are presented. Finally, a brief conclusion is presented in Sect. 5.

2 Experimental procedure

The experimental measurement of the ^{63}Cu(γ, n) cross-section was conducted at SLEGS of the SSRF, which produces γ beams within the GDR energy range from the single-neutron separation energy (S_n=10.86 MeV) to the double-neutron separation energy (S_{2n}=19.74 MeV). The experimental setup is schematically illustrated in Fig. 2. An energy-tunable SLEGS γ beam was generated through a slanting LCS process, which was achieved by the interaction of the SSRF electron beam and a CO_2 laser with incident angles ranging from 20 to 160°. After collimation, the quasi-monochromatic γ-ray was guided to irradiate the ^{63}Cu target, which was positioned precisely at the geometric center of a ^{3}He flat efficiency detector (FED) array. During the experiments, the neutrons produced from the photoneutron processes were first moderated by polyethylene in the FED array and then detected by ^{3}He proportional counters. The γ beam penetrating the target was attenuated by an additional copper attenuator (naturally abundant), and its spectrum was subsequently measured using a Bismuth Germanate (BGO) detector.

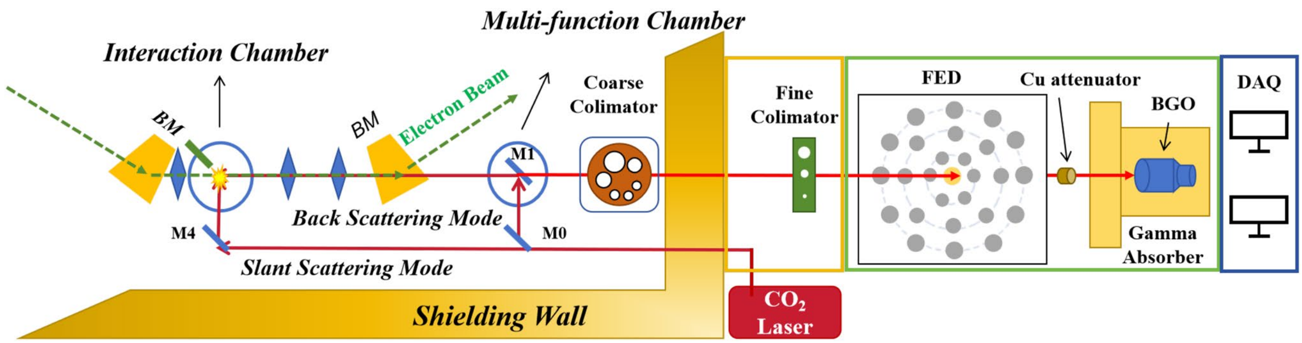

Fig. 2 (Color online) Schematic of the experimental setup for measuring the photoneutron cross-section

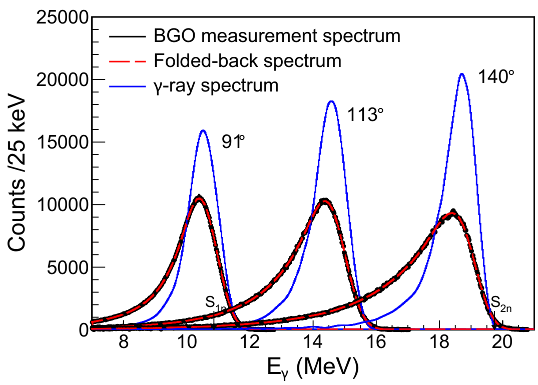

Fig. 3 (Color online) Typical γ-ray spectra measured by the BGO detector (black line), folded-back γ-ray spectra (red line), and corresponding γ-ray spectra incident on the target (blue line) at $\theta_L = 91°$, 113°, and 140°

2.1 SLEGS γ beam spectrum

In parallel with the ^{63}Cu irradiation, the γ-ray spectrum after copper attenuation was measured online using a BGO detector. Figure 3 shows an exemplary γ-ray spectrum detected at the slant-scattering angles (θ_L) of 91°, 113°, and 140°. To obtain the SLEGS γ-ray spectrum in front of the irradiation target, a direct unfolding method was employed in combination with a known response function of the BGO detector, which was obtained by a GEANT4 simulation [26]. The resulting (unfolded) γ-ray spectrum is shown in Fig. 3. The folded-back spectrum is consistent with the γ-ray spectrum measured by the detector, suggesting reliable reproduction of the γ-ray spectrum before the irradiation target. The γ-ray spectrum was integrated and corrected for the Cu attenuation factor to obtain the γ beam flux at each slant-scattering angle.

2.2 ^{63}Cu target

The diameter, thickness, and purity of the ^{63}Cu target were a 10 mm, 1.5 mm, and 99.8%, respectively. For the ^{63}Cu isotope sample, the purity of the ^{63}Cu target was determined by inductively coupled plasma–mass spectrometry. The uncertainty of the thickness was estimated to be 0.01 mm.

2.3 Neutron detection

The number of (γ, n) reactions was determined by detecting the reaction neutrons using the calibrated FED, which comprised 26 sets of ^{3}He proportional counters embedded in a polyethylene moderator. The proportional counters were arranged in three concentric rings positioned 65 mm, 110 mm, and 175 mm from the beam axis. All the sensitive volumes of the ^{3}He proportional counters were cylindrical in shape with the same length of 500 mm and inflated with ^{3}He gas at 2 atm. While the counters in Ring-1 (inner ring) were 1 inch in diameter, those in Ring-2 (middle ring) and Ring-3 (outer ring) were 2 inches in diameter. The bodies of ^{3}He proportional counters were made of stainless steel for a lower α emission rate. The inner polyethylene moderator was 450 mm × 450 mm × 550 mm (along the beam direction) and was surrounded by additional polyethylene plates with cadmium to suppress the background neutrons [27]. These background neutrons were subtracted from the duty cycle of the laser pulse. In our experiments, the duty cycle is set to 50 μs per laser period of 1000 μs. The polyethylene moderation effect significantly broadened the time distribution of the neutrons detected by the ^{3}He proportional counters. However, a flat interval of the time distribution that was only contributed by background neutrons was identifiable. Then, the number of neutrons (N_n) was directly extracted by subtracting the time-normalized background. Further details are available in [28].

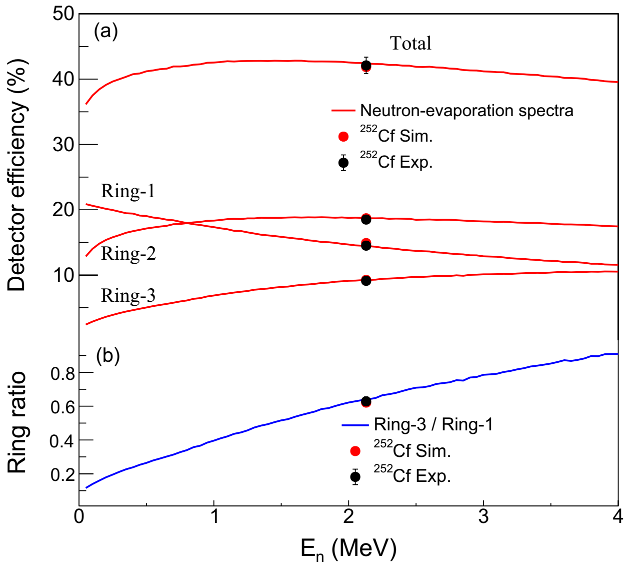

Fig. 4 (Color online) **a** Total detector efficiency and the efficiencies of individual rings. The detector efficiency curves were simulated by neutron evaporation spectra. The red dots are given by the neutron spectrum described by the Maxwell–Boltzmann distribution, $P(E) \propto E^{1/2} \cdot \exp(-E/T)$, at the average neutron energy ($T = 1.42$ MeV) of ^{252}Cf. **b** Ring-ratio curve of the FED

The average energy of the reaction neutrons was obtained using the "ring-ratio technique" originally developed by Berman and Fultz [29] and used to determine the detection efficiency. Figure 4a shows the simulated efficiency curve by GEANT4 with realistic detector configuration. For the neutron evaporation spectra, the total detector efficiency increases from 35.64% at 50 keV to 42.32% at 1.65 MeV and then falls slowly to 39.05% at 4 MeV. The efficiency calibrated using a ^{252}Cf source was 42.10 ± 1.25%, corresponding to an average neutron energy of 2.13 MeV. In our experiments, we used the ring-ratio technique to obtain the average energy of neutrons produced by (γ, n) reactions and then estimated the detector efficiency using its calibrated curve of the detector efficiency. The curve for the efficiency ratio of Ring-3 to Ring-1 is illustrated in Fig. 4b [28].

3 Data analysis and results

3.1 Monochromatic cross-section

The experimental formula for the photoneutron cross-section is given by [30, 31]

$$\int_{S_\mathrm{n}}^{E_\mathrm{max}} n_\gamma(E_\gamma)\sigma(E_\gamma)\mathrm{d}E_\gamma = \frac{N_\mathrm{n}}{N_\gamma N_\mathrm{t} \xi \epsilon_\mathrm{n} g}, \tag{1}$$

where $n_\gamma(E_\gamma)$ is the spectral distribution of the normalized LCS γ beam; $\sigma(E_\gamma)$ is the photoneutron cross-section; N_n is the number of neutrons detected; N_t is the number of target nuclei per unit area; N_γ is the number of γ-rays incident on the target; ϵ_n is the neutron detection efficiency; and $\xi = (1 - e^{\mu d})/\mu d$ is a correction factor for a thick-target measurement. Here μ is the linear attenuation coefficient of γ photons in a target of thickness d. The factor g represents the fraction of γ flux above the neutron threshold S_n:

$$g = \frac{\int_{S_\mathrm{n}}^{E_\mathrm{max}} n_\gamma(E_\gamma)\mathrm{d}E_\gamma}{\int_0^{E_\mathrm{max}} n_\gamma(E_\gamma)\mathrm{d}E_\gamma}. \tag{2}$$

The incident γ energy distribution was used to determine the cross-section $\sigma(E_\gamma)$, which is a function of the γ energy E_γ. Specifically, the incoming γ beam spectra were used to determine $n_\gamma(E_\gamma)$. The γ-energy distribution was normalized to unity: $\int_{S_\mathrm{n}}^{E_\mathrm{max}} n_\gamma(E_\gamma)\mathrm{d}E_\gamma = 1$. The measured $\sigma_\mathrm{exp}^{E_\mathrm{max}}$ for an incoming γ beam with maximum energy E_max is given by the convoluted cross-section:

$$\sigma_\mathrm{exp}^{E_\mathrm{max}} = \int_{S_\mathrm{n}}^{E_\mathrm{max}} n_\gamma(E_\gamma)\sigma(E_\gamma)\mathrm{d}E_\gamma = \frac{N_\mathrm{n}}{N_\gamma N_\mathrm{t} \xi \epsilon_\mathrm{n} g}. \tag{3}$$

Therefore, we refer to the quantity on the right side of Eq. (3) as the monochromatic cross-section. However, owing to the energy spread of the LCS γ beam (Fig. 3), the monochromatic approximation cannot be used to describe the real photoneutron cross-section.

3.2 Unfolded cross-section

The deconvoluted E_γ-dependent photoneutron cross-section, $\sigma(E_\gamma)$, must be extracted from the integral of Eq. (3). Each measurement characterized by E_max corresponds to the folding of $\sigma(E_\gamma)$ with the measured beam profile $n_\gamma(E_\gamma)$. Following Ref. [32], we unfold $\sigma(E_\gamma)$ according to Eq. (3):

$$\sigma_\mathrm{f} = \mathbf{D}_\sigma, \tag{4}$$

where σ_f represents the folded cross-section with beam profile $\mathbf{D}$. The indices i and j of matrix element $\mathbf{D}_{ij}$ correspond to E_max and E_γ, respectively. The set of equations is given by:

$$\begin{bmatrix} \sigma_1 \\ \sigma_2 \\ \vdots \\ \sigma_N \end{bmatrix}_\mathrm{f} = \begin{bmatrix} D_{11} & D_{12} & \cdots & \cdots & D_{1M} \\ D_{21} & D_{22} & \cdots & \cdots & D_{2M} \\ \vdots & \vdots & \vdots & \vdots & \vdots \\ D_{N1} & D_{N2} & \cdots & \cdots & D_{NM} \end{bmatrix} \begin{bmatrix} \sigma_1 \\ \sigma_2 \\ \vdots \\ \vdots \\ \sigma_M \end{bmatrix}. \tag{5}$$

Each row of $\mathbf{D}$ corresponds to the γ beam profile corresponding to E_max. The σ vector $[\sigma_i]_\mathrm{f}$ (i=1, 2, 3..., N) on the left-hand side of Eq. (5) is the folded cross-section, referred to as the experimental monochromatic cross-section, whereas the vector $[\sigma_j]$ (j=1,2,3..., M) on the right-hand side is the unfolded cross-section to be determined. In the present experiment, the number of monochromatic cross-sections was N=44. The energy profile of the γ beam was simulated in M=200 energy bins. The number of unfolded cross-sections was equal to M. Figure 3 presents a visual representation of the response matrix **D** for the case of ^{63}Cu. There are N=44 γ-beam spectra, and only three are shown as blue lines in Fig. 3 as examples. As the system of linear equations in Eq. (5) is under-determined, the σ_j vector cannot be obtained by matrix inversion. We determined σ_j using an iterative folding method, which can be summarized as follows:

(1) As our starting point, we choose a constant trial function σ^0 for the zeroth iteration. This initial vector is multiplied by **D** to obtain the zeroth folded vector $\sigma_{\rm f}^0 = \mathbf{D}\sigma^0$.

(2) The next trial input function, σ^1, is established by adding the difference between the experimentally measured spectrum $\sigma_{\rm exp}$ and folded spectrum $\sigma_{\rm f}^0$ to σ^0. To add the folded and input vectors, we first perform a spline interpolation on the folded vector and then interpolate to ensure that the two vectors have equal dimensions. The new input vector is

$$\sigma^1 = \sigma^0 + (\sigma_{\rm exp} - \sigma_{\rm f}^0). \tag{6}$$

(3) The above steps are iterated i times, yielding

$$\sigma_{\rm f}^i = \mathbf{D}\sigma^i, \tag{7}$$

and

$$\sigma^{i+1} = \sigma^i + (\sigma_{\rm exp} - \sigma_f^i), \tag{8}$$

until convergence is achieved. Thus, $\sigma_{\rm f}^{i+1} \approx \sigma_{\rm exp}$ is within the statistical uncertainties. To check the convergence quantitatively, we calculated the reduced χ^2 of $\sigma_{\rm f}^{i+1}$ and $\sigma_{\rm exp}$ after each iteration. The experiment was terminated when the reduced χ^2 value approached unity.

Figure 5 shows the monochromatic $\sigma_{\rm exp}^{E_{\rm max}}$ and unfolded $\sigma(E_\gamma)$ for ^{63}Cu(γ, n) reaction. Table 1 lists the $\sigma(E_\gamma)$ values

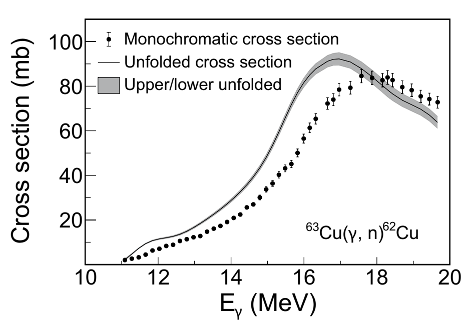

Fig. 5 (Color online) ^{63}Cu(γ,n) reaction cross-section as a function of the incident γ energy, E_γ. The dots indicate the monochromatic cross-section, while the line with the shadow area indicates the unfolded cross-section

at $E_{\rm max}$ and their uncertainties respectively. According to Eq. (3), the statistical uncertainty is primarily induced by $N_{\rm n}$. Because the incident γ-ray count was sufficiently high, its statistical uncertainty was negligible. The methodological uncertainty was approximately 1.8%, which was induced by the extraction algorithm $N_{\rm n}$ (1.5%) and unfolding methodology incorporating the simulated BGO response matrix (~1%). The systematic uncertainty was estimated to be 3.15%. This was due to the neutron detector efficiency (3.02%), γ flux attenuation and incident γ spectrum unfolding (0.90%), and target areal density (0.10%). In our study, the total uncertainty included statistical, systematic, and methodological uncertainties. The unfolded $\sigma(E_\gamma)$ had a total uncertainty of approximately 4%, except for the γ-energy region with $\sigma(E_\gamma)$ less than 7.5 mb (i.e., $S_{\rm n} < E_\gamma < 11.5$ MeV).

4 Discussion

4.1 ^{63}Cu(γ, n) reaction cross-section

Here, we compare our measurements with available experimental [4, 6–9] and evaluated [33] data. The results are presented in Fig. 6. The uncertainty of our unfolded cross-sections is comparable to those of Fultz et al. [7] and Sund et al. [9] with monochromatic photons obtained from positron annihilation in flight. Moreover, it was significantly better than those of Owen et al. [8], Berman et al. [6] and Plaisir et al. [4] obtained with bremsstrahlung radiation. Our measurements are consistent with the data of Berman et al. [6], although the latter have only a few data points. Moreover, our data agree well with those of other groups when $S_{\rm n} < E_\gamma <$15 MeV. However, our data were visibly higher than those of other studies at $E_\gamma >$ 15 MeV.

The integral ratio of two cross-section curves reflects their systematic differences [34]. The total cross-section integrated over the energy region of interest is defined as follows:

$$\sigma^{\rm int} = \int_{E_{\rm min}}^{E_{\rm max}} \sigma(E_\gamma){\rm d}E_\gamma. \tag{9}$$

We conducted experimental measurements on ^{197}Au(γ, n) and ^{159}Tb(γ, n) reactions at SLEGS [28]. The ^{197}Au(γ, n) reaction data were compared with those reported by Itoh et al. [30]. The resulting $\sigma^{\rm int}$ difference was ~ 0.4%, suggesting the reliability of SLEGS in the measurement procedure and data analysis [28]. We calculated $\sigma^{\rm int}$ of ^{63}Cu(γ, n) reactions for different laboratories within

Table 1 Unfolded cross-sections and corresponding uncertainties for $^{63}Cu(\gamma, n)^{62}Cu$

E_γ (MeV)	σ (mb)	Statistical uncertainty (mb)	Methodological uncertainty (mb)	Systematic uncertainty (mb)	Total uncertainty (mb)
11.09	2.18	0.40	0.03	0.06	0.41
11.28	4.70	0.23	0.05	0.08	0.25
11.47	7.28	0.13	0.06	0.10	0.17
11.66	9.37	0.12	0.08	0.14	0.20
11.85	10.74	0.10	0.11	0.20	0.25
12.03	11.51	0.11	0.12	0.22	0.28
12.22	12.02	0.08	0.16	0.26	0.32
12.41	12.63	0.09	0.15	0.28	0.33
12.60	13.57	0.09	0.18	0.33	0.39
12.78	14.90	0.10	0.19	0.36	0.42
12.97	16.55	0.10	0.21	0.39	0.45
13.16	18.42	0.09	0.21	0.40	0.46
13.34	20.43	0.09	0.24	0.46	0.53
13.53	22.56	0.11	0.26	0.51	0.58
13.71	24.80	0.12	0.28	0.55	0.62
13.89	27.20	0.12	0.31	0.60	0.69
14.07	29.78	0.14	0.33	0.66	0.75
14.25	32.62	0.15	0.36	0.71	0.81
14.43	35.74	0.17	0.40	0.81	0.92
14.61	39.30	0.19	0.44	0.85	0.97
14.79	43.35	0.19	0.49	0.95	1.08
14.96	48.06	0.22	0.54	1.06	1.21
15.14	53.50	0.21	0.59	1.15	1.31
15.31	59.48	0.25	0.65	1.27	1.45
15.48	65.73	0.25	0.70	1.36	1.55
15.66	71.74	0.30	0.73	1.42	1.63
15.82	77.12	0.32	0.79	1.58	1.79
15.99	81.53	0.30	0.92	1.78	2.03
16.16	85.05	0.31	0.99	1.93	2.20
16.32	87.75	0.32	1.09	2.06	2.35
16.65	91.18	0.34	1.24	2.28	2.62
16.81	92.06	0.47	1.23	2.33	2.68
16.96	92.23	0.42	1.28	2.47	2.82
17.27	90.85	0.40	1.28	2.50	2.84
17.58	87.90	0.38	1.40	2.67	3.04
17.87	84.20	0.31	1.43	2.64	3.02
18.15	80.26	0.42	1.47	2.61	3.02
18.29	78.33	0.43	1.54	2.65	3.09
18.43	76.55	0.42	1.42	2.61	3.00
18.70	73.70	0.36	1.32	2.51	2.86
18.95	71.67	0.45	1.28	2.47	2.81
19.20	69.68	0.42	1.27	2.38	2.73
19.44	67.06	0.34	1.26	2.34	2.68
19.67	63.70	0.32	1.31	2.30	2.66

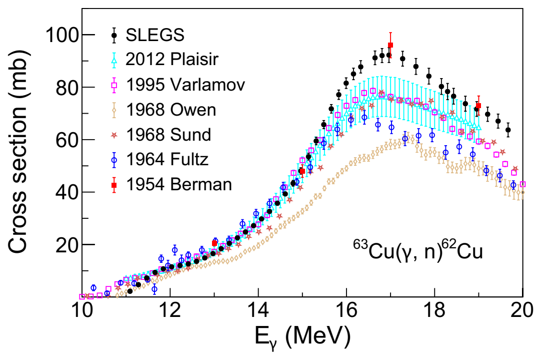

Fig. 6 (Color online) Unfolded cross-section curve for ^{63}Cu(γ, n) together the available experimental and evaluated data [4, 6–9, 33]

Table 2 Integrated ^{63}Cu(γ, n) cross-section data

Author	σ^{int} (mb)	
	[S_{1n}, 15 MeV]	[15 MeV, S_{2n}]
This work	83.25	369.27
Plaisir et al. [4]	86.49	277.66
Varlamov et al. [33]	93.08	320.18
Owen et al. [8]	60.21	239.32
Sund et al. [9]	76.90	318.37
Fultz et al. [7]	93.76	284.52

$S_{1n} < E_\gamma < 15$ MeV and 15 MeV $< E_\gamma < S_{2n}$. The results are shown in Table 2. For $S_{1n} < E_\gamma <$15 MeV, the relative difference between the σ^{int} value and those of the others is 4–13%, except for the data of Owen, for which the difference is 28%. In contrast, for 15 MeV $< E_\gamma < S_{2n}$, our data are larger than the others by a factor of 0.13 −0.35. Table 2 shows that the data of Owen are evidently lower than the others within the two aforementioned energy regions. Consequently, it is not a priority. Overall, our measurements are expected to clarify the inconsistency between the available experimental data for the ^{63}Cu(γ, n) reaction.

4.2 Radiative ^{62}Cu(n, γ) cross-section

γSF [35, 36] is a statistical quantity employed in the Hauser–Feshbach model of the compound nuclear reaction. The γSF in the de-excitation mode aids in determining the radiative (n, γ) cross-sections that are directly relevant to the s-process nucleosynthesis of elements heavier than iron. The downward γSF for dipole radiation at a given energy E_γ is defined as [37]

$$\overleftarrow{f_{X1}}(E_\gamma) = E_\gamma^{-3}\frac{\langle\Gamma_{X1}(E_\gamma)\rangle}{D_\ell}. \tag{10}$$

Here X is either electric (E) or magnetic (M); $\langle\Gamma_{X1}(E_\gamma)\rangle$ is the average radiation width; and D_ℓ is the average level spacing for s-wave ($\ell = 0$) or p-wave ($\ell = 1$) neutron resonances.

In contrast, γSF in the excitation mode for dipole radiation [37] is defined by the average cross-section for $E1/M1$ photoabsorption $\sigma_{X1}(E_\gamma)$ to the final states with all possible spins and parities [36]:

$$\overrightarrow{f_{X1}}(E_\gamma) = \frac{E_\gamma^{-1}}{g_J(\pi\hbar c)^2}\langle\sigma_{X1}(E_\gamma)\rangle. \tag{11}$$

Here, the spin factor $g_J = (2J+1)/(2J_0+1)$, where $J = 1$ and $J_0 = 0$ (ground state).

Above the neutron separation energy, except at energies near the neutron threshold, the total upward γSF can be determined by substituting $\sigma_{X1}(E_\gamma)$ with the experimental (γ, n) cross-sections that dominate the photoabsorption cross-sections. According to the principle of detailed balance [38] and the generalized Brink hypothesis, the equality of the upward and downward γSF, $f_{X1}(E_\gamma) = \overleftarrow{f_{X1}}(E_\gamma) = \overrightarrow{f_{X1}}(E_\gamma)$, connect the (upward) ($\gamma$, n) cross-section $\sigma_{\gamma n}$ to the (downward) γSF by [37]

$$f_{X1}(E_\gamma) = \frac{1}{g_J\pi^2\hbar^2c^2}\frac{\sigma_{\gamma n}(E_\gamma)}{E_\gamma}, \tag{12}$$

where $1/g_J\pi^2\hbar^2c^2 = 8.674\times10^{-8}\,\text{mb}^{-1}\text{MeV}^{-2}$. This relation yields the experimentally constrained γSF from the measured ^{63}Cu(γ, n) reaction data, as indicated by the red dots in Fig. 7.

In TALYS (version 1.96) [39, 40], various phenomenological and microscopic models have been established to describe the γSF. The Brink–Axel Lorentzian model and simple modified Lorentzian (SMLO) model [41] for the $E1$ strength closely

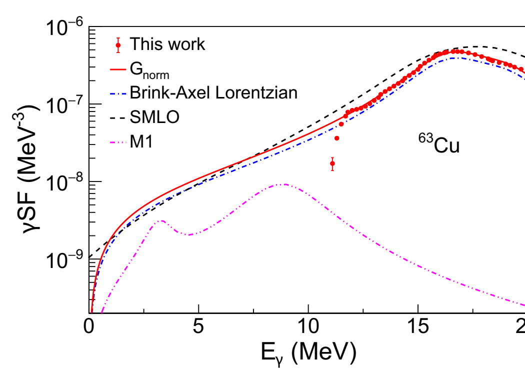

Fig. 7 (Color online) Comparison of the γSF of ^{63}Cu calculated using the Brink–Axel Lorentzian model (blue dashed line) and SMLO model (black dashed line) for the $E1$ strength in TALYS with the γSF extracted from our data (red dots). γSF values (red solid line) optimized using G_{norm}. The spin-flip and scissor model for the $M1$ strength is indicated by the pink dashed line

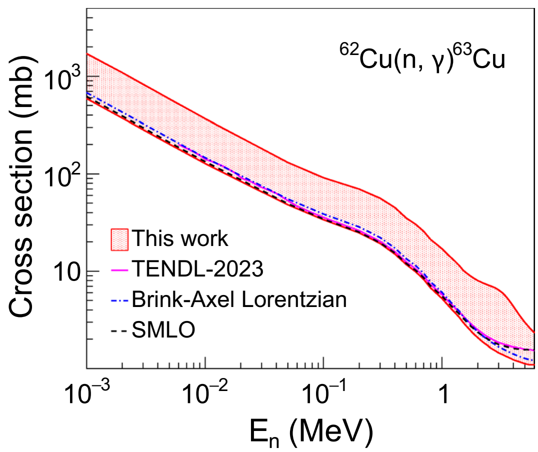

Fig. 8 (Color online) ^{62}Cu(n, γ) cross-section calculated with TALYS code based on the Brink–Axel Lorentzian model with G_{norm} optimization. The theoretical uncertainty corresponds to the use of different NLD models [39, 40]. Additional TALYS calculations based on the Brink–Axel Lorentzian model (blue line) and the SMLO model (black line) without G_{norm} optimization as well as TENDL-2023 evaluations [45] (pink line) are also shown for comparison

approximate the experimental values. The blue and black lines in Fig. 7 represent the γSFs calculated using the aforementioned two models. The pink lines in Fig. 7 show the spin-flip and scissor model of the $M1$ strength [42]. Although these two models have contributed to advancements in calculating the γ SF, discrepancies between model predictions and experimental observations remain. To improve the predictive accuracy of these models, we refined the Brink–Axel Lorentzian model by incorporating the normalization factor G_{norm} for γSF available in TALYS. G_{norm} was optimized by minimizing χ^2 and aligning the theoretical calculations of the γSF more closely with the experimental data. The expression for χ^2 is given by

$$\chi^2 = \frac{1}{N}\sum_{i=1}^{N}\left(\frac{\sigma_{\text{th},i} - \sigma_{\text{exp},i}}{\sigma_{\text{err},i}}\right)^2, \quad (13)$$

where N represents the total number of experimental data points, and $\sigma_{\text{th},i}$, $\sigma_{\text{exp},i}$, and $\sigma_{\text{err},i}$ denote the theoretical value, experimental data, and experimental error of the γSF for the i-th data point, respectively. By adjusting G_{norm}, we find that the χ^2 value reaches a minimum of 1.46 when G_{norm} = 1.2. The red solid line in Fig. 7 represents the optimized γSF values, demonstrating closer agreement with the experimental data.

The radiative (n, γ) cross-section strongly depends on the γSF and is sensitive to the nuclear level density (NLD) model employed. We extracted the experimentally constrained γSF from our newly measured ^{63}Cu(γ, n) reaction data and then optimized the Brink–Axel Lorentzian model for $E1$ strength in TALYS using G_{norm}. Finally, the radiative (n, γ) cross-section for ^{62}Cu was calculated based on the Brink–Axel Lorentzian model with G_{norm} optimization. The results are presented in Fig. 8 as the red band. The spin-flip and scissor model of the $M1$ strength was considered in the TALYS calculations. The theoretical uncertainty corresponds to the use of six NLD models [40]. A similar study was performed by Utsunomiya et al. [43], in which radiative (n, γ) cross-sections of ^{136,137}Ba isotopes were obtained. In our study, owing to the lack of experimental data on ^{63}Cu in terms of low-lying excited levels and neutron resonance spacings, we could not effectively constrain the NLD model. Consequently, a relatively large theoretical uncertainty was obtained. To reduce the theoretical uncertainty of the (n, γ) cross-sections, both the γSF and NLD models should be effectively constrained. A good example can be found in Renstrom et al. [44], in which charged particle-induced reaction data were used to constrain the NLD model.

To further investigate the ^{62}Cu(n, γ) cross-section, additional TALYS calculations based on the Brink–Axel Lorentzian and SMLO models were performed without G_{norm} optimization. The calculated results and available TENDL-2023 evaluations [45] are also presented in Fig. 8 for comparison, which shows a good agreement between each other. To the best of our knowledge, this is the first time that the experimentally constrained ^{62}Cu(n, γ) cross-section has been obtained. This supports the principle of detailed balance and generalized Brink hypothesis for ^{63}Cu isotope.

5 Conclusion

We performed new measurements on the ^{63}Cu(γ, n) cross-section at energies below S_{2n} with quasi-monochromatic and energy-tunable SLEGS γ beams. Using the unfolding iteration method, the ^{63}Cu(γ, n) reaction data were obtained within the energy range of 11.1−19.7 MeV, and the resulting uncertainty was controlled within 4%. The comparison between our measurement and previously available experimental and evaluated cross-sections was discussed, helping in resolving a long-standing discrepancy between the existing ^{63}Cu(γ, n) reaction data. Based on these new data, the experimentally constrained γSF for ^{63}Cu was extracted, which was reasonably consistent with the TALYS calculations when considering different γSF models. Furthermore, the cross-sectional curve of the inverse reaction, ^{62}Cu(n, γ), was obtained for the first time. Our calculations provide an alternative for extracting the (n, γ) cross-sections for some unstable nuclides.

Acknowledgements We thank the SSRF operating team for their support of this study. We are grateful to Professor H. Utsunomiya of Konan University, Japan, for useful suggestions and discussions.

Author contributions All authors contributed to the study conception and design. Material preparation, data collection, and analysis were performed by Zhi-Cai Li, Zi-Rui Hao, Qian-kun Sun, Yu-Long Shen, Long-Xiang Liu, Hang-Hua Xu, Yue Zhang, Pu Jiao, Meng-Die Zhou, Yu-Xuan Yang, Sheng Jin, Kai-Jie Chen, Zhen-Wei Wang, Shan Ye, Xin-Xiang Li, Chun-Wang Ma, Hong-Wei Wang, Gong-Tao Fan, and Wen Luo. The first draft of the manuscript was written by Zhi-Cai Li, and all authors commented on the previous versions of the manuscript. All authors read and approved the final manuscript.

Declarations

Conflict of interest Chun-Wang Ma and Hong-Wei Wang are the editorial board members for Nuclear Science and Techniques and were not involved in the editorial review, or the decision to publish this article. All authors declare that there are no conflict of interest.

Data availability statement The data that support the findings of this study are openly available in Science Data Bank at https://cstr.cn/31253.11.sciencedb.j00186.00452 and https://doi.org/10.57760/sciencedb.j00186.00452.

References

1. M.A. Green, C.J. Mathias, M.J. Welch et al., Copper-62-labeled pyruvaldehyde bis (n4-methylthiosemicarbazonato) copper (ii): synthesis and evaluation as a positron emission tomography tracer for cerebral and myocardial perfusion. J. Nucl. Med. **31**, 1989–1996 (1990). https://doi.org/10.1097/00004424-199012000-00013
2. W. Luo, Production of medical radioisotope ^{64}Cu by photoneutron reaction using ELI-NP γ-ray beam. Nucl. Sci. Tech. **27**, 96 (2016). https://doi.org/10.1007/s41365-016-0094-6
3. W. Luo, D.L. Balabanski, D. Filipescu, A data-based photonuclear simulation algorithm for determining specific activity of medical radioisotopes. Nucl. Sci. Tech. **27**, 113 (2016). https://doi.org/10.1007/s41365-016-0111-9
4. C. Plaisir, F. Hannachi, F. Gobet et al., Measurement of the ^{85}Rb(γ, n)^{84m}Rb cross-section in the energy range 10–19 MeV with bremsstrahlung photons. Eur. Phys. J. A **48**, 68 (2012). https://doi.org/10.1140/epja/i2012-12068-7
5. Z.C. Li, Y.X. Yang, W. Luo, et al., Fast measurement of quasmonochromatic MeV γ-beam flux using ^{63}Cu(γ, n)^{62}Cu reaction at Shanghai laser electron gamma source. Nucl. Instr. and Meth. B **559**, 165595 (2025). https://doi.org/10.1016/j.nimb.2024.165595
6. A.I. Berman, K.L. Brown, Absolute cross section versus energy of the ^{63}Cu(γ, n) and ^{63}Cu(γ, 2n) reactions. Phys. Rev. **96**, 83 (1954). https://doi.org/10.1103/PhysRev.96.83
7. S. Fultz, R. Bramblett, J. Caldwell et al., Photoneutron cross sections for natural Cu, ^{63}Cu, and ^{65}Cu. Phys. Rev. **133**, B1149 (1964). https://doi.org/10.1103/PhysRev.133.B1149
8. D. Owen, E. Muirhead, B. Spicer, Structure in the giant resonance of ^{64}Zn and ^{63}Cu. Nucl. Phys. A **122**, 177–183 (1968). https://doi.org/10.1016/0375-9474(68)90711-2
9. R. Sund, M. Baker, L. Kull et al., Measurements of the ^{63}Cu(γ, n) and (γ, 2n) cross sections. Phys. Rev. **176**, 1366 (1968). https://doi.org/10.1103/PhysRev.176.1366
10. M. Martins, E. Hayward, G. Lamaze et al., Experimental test of the bremsstrahlung cross section. Phys. Rev. C **30**, 1855 (1984). https://doi.org/10.1103/PhysRevC.30.1855
11. M. Antunes, M. Martins, Two proton and two neutron photoemission cross sections of ^{63}Cu. Phys. Rev. C **52**, 1484 (1995). https://doi.org/10.1103/PhysRevC.52.1484
12. A. Varlamov, V. Varlamov, D. Rudenko et al., Atlas of giant dipole resonances. Parameters and graphs of photonuclear reaction cross sections. Tech. Rep. International Atomic Energy Agency. International Nuclear Data Committee (1999)
13. V. Varlamov, A. Davydov, M. Makarov et al., Reliability of the data on the cross sections of the partial photoneutron reaction for ^{63,65}Cu and ^{80}Se nuclei. Bull. Russ. Acad. Sci. Phys. **80**, 317–324 (2016). https://doi.org/10.3103/S1062873816030333
14. A.I. Blokhin, M.B. Chadwick, T. Fukahori, et al., Handbook on photonuclear data for applications. Cross Sections and Spectra. IAEA-TECDOC-1178
15. T. Kawano, Y. Cho, P. Dimitriou et al., IAEA photonuclear data library 2019. Nucl. Data Sheets **163**, 109–162 (2020). https://doi.org/10.1016/j.nds.2019.12.002
16. V. Varlamov, B. Ishkhanov, V. Orlin et al., Evaluated cross sections of the $\sigma(\gamma$, nX) and $\sigma(\gamma$, 2nX) reactions on ^{112,114,116,117,118,119,120,122,124}Sn isotopes. Bull. Russ. Acad. Sci. Phys. **74**, 833–841 (2010). https://doi.org/10.3103/S1062873810060225
17. V. Varlamov, B. Ishkhanov, V. Orlin et al., New data for the ^{197}Au(γ, nX) and ^{197}Au (γ, 2nX) reaction cross sections. Bull. Russ. Acad. Sci. Phys. **74**, 842–849 (2010). https://doi.org/10.3103/S1062873810060237
18. Z.C. Li, Y. Yang, Z.W. Cao et al., Effective extraction of photoneutron cross-section distribution using gamma activation and reaction yield ratio method. Nucl. Sci. Tech. **34**, 170 (2023). https://doi.org/10.1007/s41365-023-01330-z
19. W. Luo, W. Xu, Q.Y. Pan et al., A 4D Monte Carlo laser-compton scattering simulation code for the characterization of the future energy-tunable SLEGS. Nucl. Instr. Meth. A **660**, 108–115 (2011). https://doi.org/10.1016/j.nima.2011.09.035
20. H.H. Xu, G.T. Fan, H.L. Wu et al., Interaction chamber design for an energy continuously tunable sub-MeV laser-compton gamma-ray source. IEEE Trans. Nucl. Sci. **63**, 906–912 (2016). https://doi.org/10.1109/TNS.2015.2496256
21. H.W. Wang, G.T. Fan, L.X. Liu et al., Development and prospect of Shanghai laser compton scattering gamma source. Nucl. Phys. Rev. **37**, 53–63 (2020). https://doi.org/10.11804/NuclPhysRev.37.2019043
22. H.W. Wang, G.T. Fan, L.X. Liu et al., Commissioning of laser electron gamma beamline SLEGS at SSRF. Nucl. Sci. Tech. **33**, 87 (2022). https://doi.org/10.1007/s41365-022-01076-0
23. J.H. He, Z.T. Zhao et al., Shanghai synchrotron radiation facility. Natl. Sci. Rev. **1**, 171 (2014). https://doi.org/10.1093/nsr/nwt039
24. Z.R. Hao, G.T. Fan, H.W. Wang et al., A new annular collimator system of SLEGS beamline at Shanghai light source. Nucl. Instrum. Methods Phys. Res. B **519**, 9–14 (2022). https://doi.org/10.1016/j.nimb.2022.02.010
25. H.H. Xu, G.T. Fan, H.W. Wang et al., Interaction chamber for laser compton slant-scattering in SLEGS beamline at Shanghai light source. Nucl. Instrum. Methods Phys. Res. A **1033**, 166742 (2022). https://doi.org/10.1016/j.nima.2022.166742
26. L.X. Liu, H. Utsunomiya, G.T. Fan et al., Energy profile of laser compton slant-scattering γ-ray beams determined by direct unfolding of total-energy responses of a BGO detector. Nucl. Instrum. Methods Phys. Res. Sect. A **1063**, 169314 (2024). https://doi.org/10.1016/j.nima.2024.169314
27. Z.R. Hao, G.T. Fan, L.X. Liu et al., Design and simulation of 4π flat-efficiency ^{3}He neutron detector array. Nuclear Techniques (in Chinese) **43**, 110501 (2020). https://doi.org/10.11889/j.0253-3219.2020.hjs.43.110501

28. Z.R. Hao, L.X. Liu, Y. Zhang et al., Photoneutron dataset generation and analysis at SLEGS. ChinaXiv:202412.00386 https://doi.org/10.12074/202412.00386
29. B.L. Berman, S. Fultz, Measurements of the giant dipole resonance with monoenergetic photons. Rev. Mod. Phys. **47**, 713 (1975). https://doi.org/10.1103/RevModPhys.47.713
30. O. Itoh, H. Utsunomiya, H. Akimune et al., Photoneutron cross sections for Au revisited: measurements with laser compton scattering γ-rays and data reduction by a least-squares method. J. Nucl. Sci. Technol. **48**, 834–840 (2011). https://doi.org/10.1080/18811248.2011.9711766
31. D. Filipescu, I. Gheorghe, H. Utsunomiya et al., Photoneutron cross sections for samarium isotopes: toward a unified understanding of (γ, n) and (n, γ) reactions in the rare earth region. Phys. Rev. C **90**, 064616 (2014). https://doi.org/10.1103/PhysRevC.90.064616
32. H. Utsunomiya, T. Renstrøm, G.M. Tveten et al., Photoneutron cross sections for Ni isotopes: toward understanding (n, γ) cross sections relevant to weak s-process nucleosynthesis. Phys. Rev. C **98**, 054619 (2018). https://doi.org/10.1103/PhysRevC.98.054619
33. V.V. Varlamov, N.G. Efimkin, B.S. Ishkhanov et al., Evaluation of Cu-64,65(γ, np) and Cu-63,65(γ, p) reaction cross sections in the energy range of giant dipole resonance and isospin splitting of the GDR of Cu nuclei. Bull. Rus. Acad. Sci. Phys. **59**, 911 (1995)
34. V. Varlamov, B. Ishkhanov, V. Orlin, Reliability of (γ, 1n),(γ, 2n), and (γ, 3n) cross-section data on Tb-159. Phys. Rev. C **95**, 054607 (2017). https://doi.org/10.1103/PhysRevC.95.054607
35. G. Bartholomew, E. Earle, A. Ferguson et al., Gamma-ray strength functions. Adv. Nucl. Phys. **7**, 229–324 (1973). https://doi.org/10.1007/978-1-4615-9044-6_4
36. J. Kristiak, E. Betàk, *Neutron induced reactions. In: Proceedings of the 4th International Symposium Smolenice, Czechoslovakia, June 1985*, Springer Science & Business Media, (2012)
37. R. Capote, M. Herman, P. Obložinskỳ et al., RIPL-reference input parameter library for calculation of nuclear reactions and nuclear data evaluations. Nucl. Data Sheets **110**, 3107–3214 (2009). https://doi.org/10.1016/j.nds.2009.10.004
38. J.M. Blatt, V.F. Weisskopf, *Theortical nuclear physics* (Wiley, New York, 1952)
39. A.J. Koning, D. Rochman, Modern nuclear data evaluation with the TALYS code system. Nucl. Data Sheets **113**, 2841–2934 (2012). https://doi.org/10.1016/j.nds.2012.11.002
40. A. Koning, S. Hilaire, S. Goriely, TALYS: modeling of nuclear reactions. Eur. Phys. J. A **59**, 131 (2023). https://doi.org/10.1140/epja/s10050-023-01034-3
41. S. Goriely, V. Plujko, Simple empirical $E1$ and $M1$ strength functions for practical applications. Phys. Rev. C **99**, 014303 (2019). https://doi.org/10.1103/PhysRevC.99.014303
42. E. Balbutsev, I. Molodtsova, P. Schuck, Spin scissors mode and the fine structure of $M1$ states in nuclei. Nucl. Phys. A **872**, 42–68 (2011). https://doi.org/10.1016/j.nuclphysa.2011.09.013
43. H. Utsunomiya, T. Renstrøm, G.M. Tveten et al., γ-ray strength function for barium isotopes. Phys. Rev. C **100**, 034605 (2019). https://doi.org/10.1103/PhysRevC.100.034605
44. T. Renstrøm, H. Utsunomiya, H.T. Nyhus et al., Verification of detailed balance for γ absorption and emission in Dy isotopes. Phys. Rev. C **98**, 054310 (2018). https://doi.org/10.1103/PhysRevC.98.054310
45. TENDL-2023 nuclear data library., https://tendl.web.psi.ch/tendl_2023/neutron_html2024/neutron.html